MRS Advances © 2019 Materials Research Society
DOI: 10.1557/adv.2019.472

Infrared Propagating Electromagnetic Surface Waves Excited by Induction

Jonathan R. Brescia[1,3] , Justin W. Cleary[2] , Evan M. Smith[2,3] , Robert E. Peale[1]

[1] *Physics, University of Central Florida, Orlando FL 32816 USA*

[2] *Air Force Research Laboratory, Sensors Directorate, RYDH, Wright-Patterson AFB OH 45433 USA*

[3] *KBRwyle, Beavercreek, OH, 45431*

Abstract

Propagating inhomogeneous electromagnetic waves called surface plasmon polaritons (SPPs) can be excited by free-space beams on corrugated conducting surfaces at resonance angles determined by corrugation period, permittivity, and optical frequency. SPPs are coupled to and co-propagate with surface charge displacements. Complete electrical isolation of individual conducting corrugations prevents the charge displacement necessary to sustain an SPP, such that excitation resonances of traveling SPPs are absent. However, SPPs can be excited via electric induction if a smooth conducting surface exists below and nearby the isolated conducting corrugations. The dependence of SPP excitation resonances on that separation is experimentally investigated here at long-wave infrared wavelengths. We find that excitation resonances for traveling SPPs broaden and disappear as the dielectric's physical thickness is increased beyond ~1% of the free-space wavelength. The resonance line width increases with refractive index and optical thickness of the dielectric.

INTRODUCTION

Concentration and confinement of electromagnetic fields via excitation of surface plasmon polaritons (SPP) has well known commercial applications in bio-sensing [1]. Generally, a coupler is required for free space optical beams to excite SPPs on conducting surfaces. The coupler used in commercial systems is the Kretschmann prism [1]. The sensing mechanism is the angular shift of an angularly sharp SPP excitation

resonance when analyte molecules bind to the surface and change the local refractive index.

Most commercial systems operate at visible or near-IR optical frequencies, but there are potential advantages to operating farther into the infrared [2,3]. However, prisms make poor long-wave-infrared couplers due in part to high indices and dispersion of suitably-transparent non-hygroscopic materials [3].

Grating couplers comprising corrugated conducting surfaces are well known for excitation of infrared traveling SPPs [4,5]. Such have been used to excite SPPs for molecular sensing by out-coupling the traveling SPP at a second grating into a free-space homogeneous wave, which can be collected by a conventional infrared detector [4]. A sensor based on changes in SPP-excitation resonance angle, as in commercial biosensors [1], on a single grating faces the challenge that any surface analyte or flow-confinement apparatus would interfere with the incident excitation beam. The analyte medium is usually aqueous, and the transmittance for a double pass through a 1 micron thick layer of water is only 30% [6]. Similar challenges would face devices that integrate sensors on the grating coupler.

SPP devices have been proposed that feature gratings in which the conducting corrugations are electrically isolated from one another and from a conducting ground plane, with sensors located below the grating [7,8]. The isolation might comprise an analyte flow channel with sensing based on changes to the resonance angles measured in reflectance, as in a conventional SPR biosensor [1]. We reported that when individually-isolated conducting corrugations are deposited on a dielectric substrate without a nearby continuous conducting surface, no excitation resonances for traveling SPPs are observed [5]. However, SPPs might be excited on a continuous conducting plane by electric induction if that plane is sufficiently near to the conducting corrugations.

This paper experimentally investigates the range of separations between grating bars and ground plane that allow observation of traveling-SPP excitation resonances in the long-wave infrared (LWIR). We find that the allowable separation is no more than ~1% of the free space wavelength for a long-wave infrared excitation beam.

We also report that the excitation resonance line width for traveling SPPs depends on the refractive index of the dielectric that isolates the grating bars from the continuous ground plane. The experiments are done in the LWIR, a spectral region of strong dispersion, and this dispersion affects the line width. The line width appears to be less dependent on dielectric extinction coefficient than on refractive index.

THEORETICAL CONSIDERATIONS

Surface plasmon polaritons (SPP) are inhomogeneous electromagnetic surface waves that are coupled to charge displacements on a conducting surface. A schematic polariton dispersion curve [5], frequency ω_{SPP} vs in-plane wavevector k_x, is presented in Figure 1, lower left. Because the SPP wave must drag along its associated charge displacement, SPPs propagate more slowly than does a homogeneous plane wave in air, whose linear dispersion curve for grazing incidence ($\theta = 90^o$) with slope c is indicated Figure 1 (lower left). The slope $d\omega_{SPP}/dk_x < c$ gives the group velocity for SPP energy propagation. The straight line with slope c never crosses the SPP dispersion curve. Thus, conversion of light to SPP on a smooth conducting surface cannot conserve momentum $\hbar k$.

If the conducting surface is corrugated, momentum can be conserved, allowing SPP excitation, by adding or subtracting integer multiples of grating momentum. Figure 1 shows two light lines with different incidence angles $\theta < 90^o$. Each line has been horizontally shifted by one unit of grating momentum $k_g = 2\pi/p$ for grating period p. For

these shifted lines, there are two intersections with the SPP curves, which determine two SPP excitation resonance frequencies for each of the two incidence angles. There are other resonances for different positive and negative multiples of k_g and for forward and backward propagating SPPs, but Figure 1 suffices to qualitatively explain the resonances studied here. For the considered metals and IR wavelengths, our actual operating conditions are far below the polariton region of the dispersion curve, in comparison to the schematic, but the general considerations still apply. The equivalent to Figure 1 using dispersion for actual silver gratings and CO_2-laser wavelengths has been presented in [5].

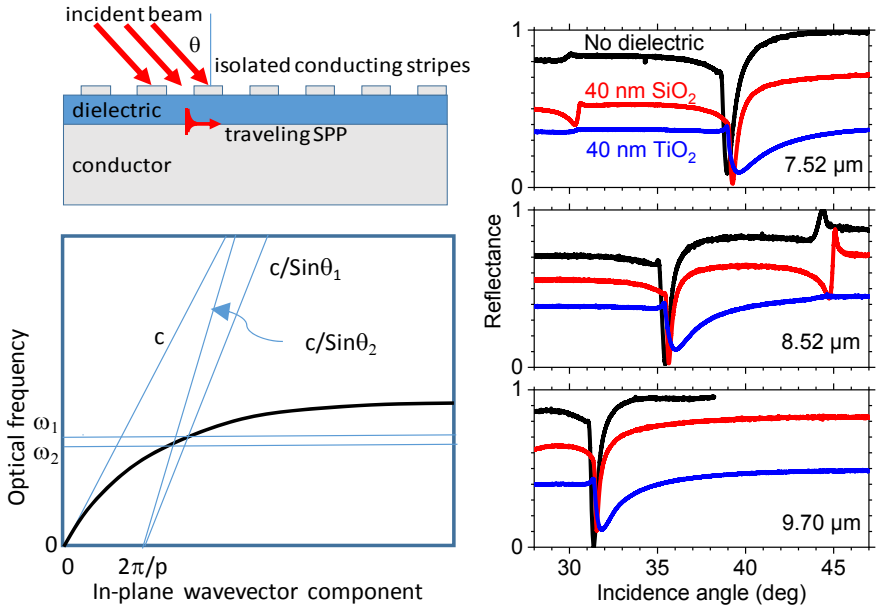

Figure 1. (left lower) Schematic SPP dispersion curve and various light lines. (left upper) Schematic SPP grating coupler with insolating dielectric layer. (right) Measured SPP excitation resonances for different dielectric layers, or no dielectric, and at three different LWIR wavelengths.

Figure 1 upper left presents a schematic of the sample geometry for this paper. Conducting grating bars are separated by a thin dielectric layer from a smooth conducting surface. Fields from the polarization in the bars, which is driven by the incident wave, in principle may excite a polarization of free electrons in the continuous conductor by electric induction. If traveling SPPs can be excited, they must propagate along the continuous interface between dielectric and metal ground plane, as shown, so that their associated surface-charge displacements can co-propagate with the SPP fields. The SPP is represented schematically by the exponentially decaying fields at the interface between the dielectric and ground plane.

EXPERIMENTAL DETAILS

The dielectrics investigated were TiO_2 and SiO_2 . These were deposited by electron beam evaporation to a thickness *t* that ranged from 0 to 640 nm. The grating had 50% duty cycle, its period was 20 μm, and the height of the deposited conducting stripes

was 1 μm [5]. Both stripes and ground plane were aluminum, and the stripes were patterned by conventional contact photolithography and metal lift-off.

SPP excitation resonances are revealed as angularly narrow dips in the specular reflection of a suitably-polarized monochromatic beam [5]. Our experiments are performed using a tunable LWIR beam from a TM-polarized quantum cascade laser (QCL). The SPP coupler is mounted on the θ spindle of a motorized θ-2θ goniometer, and an IR detector is mounted on an arm attached to the 2θ spindle. The incident QCL beam was pulsed at 100 kHz with 5% duty cycle, and the detected specular-reflected signal is synchronously lock-in amplified. The output of the lock-in is recorded as a function of incident angle using a labview program.

RESULTS

Figure 1 (right) compares angular reflectance spectra at three different wavelengths and for the two different dielectrics of thickness 40 nm to a spectrum taken on a sample with no dielectric at all. The strong resonances are due to excitation of traveling SPPs with one unit of grating momentum. The smaller features are due to SPPs excited with different units of grating momentum. The position and line shapes of all observed resonances are theoretically understood [5]. The highest baseline reflectance and sharpest resonance occurs for the zero-dielectric reference. The lowest baseline reflectance and broadest resonance occurs for the sample with TiO_2 dielectric.

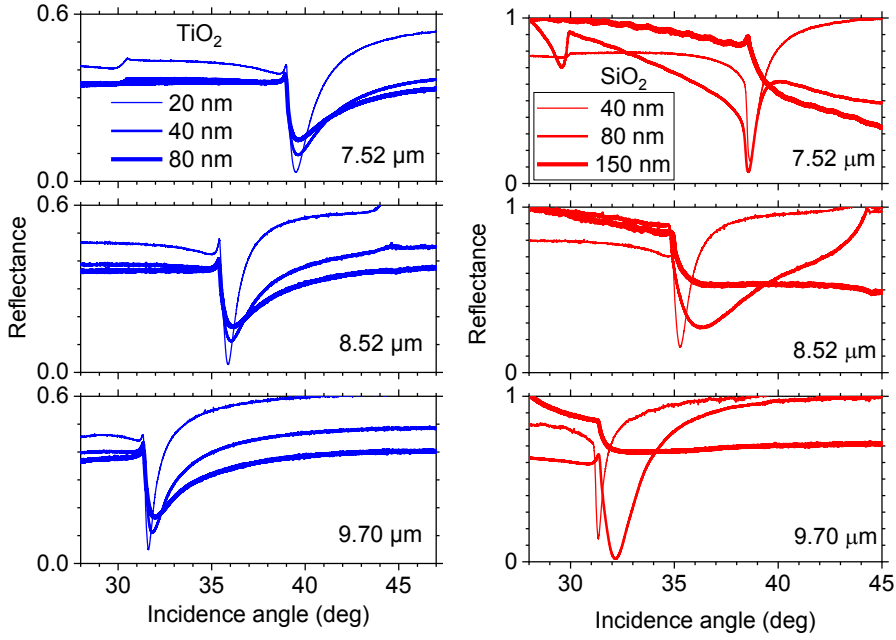

Figure 2. (left) Resonance dependence on thickness of dielectric, TiO_2 (left) and SiO_2 (right).

Figure 2 presents angular reflectance spectra for three different LWIR wavelengths and three different dielectric thicknesses. Results for TiO_2- and SiO_2-based devices are plotted in the left and right parts of Figure 2, respectively. To better reveal the

difference in line shapes, the SiO_2 data are normalized to their peak values. Resonance lines broaden with increasing dielectric thickness for all three wavelengths. For the thinnest TiO_2 sample, the resonance clearly sharpens with increasing wavelength. For SiO_2 samples the wavelength dependence is non-monotonic. Note that for samples with 40 nm of dielectric, resonances at all wavelengths for TiO_2 devices are broader than those of SiO_2 devices. For samples with 80 nm dielectric, the same holds true except at $\lambda = 8.52$ μm.

Sharp resonances are better for sensing methodologies based on shifts in resonance angle at fixed wavelength [1]. Figure 3 (symbols) presents resonance full-width at half maximum (FWHM) for devices with 20 nm TiO_2 and with 40 nm SiO_2. These thicknesses were chosen because the resonances are well defined with similar widths and line shapes for the two materials. Two samples fabricated in different facilities were analyzed for SiO_2. The gap in the data between 8.5 and 9.5 μm wavelength is due to tuning limitations of the QCL. A smaller gap occurs at 10.1 μm where the resonance of interest crosses another resonance, so that the FWHM could not be determined. Also plotted as curves are the refractive index and extinction coefficient spectra for the two dielectrics from [9], which were obtained from ellipsometry of similarly deposited films.

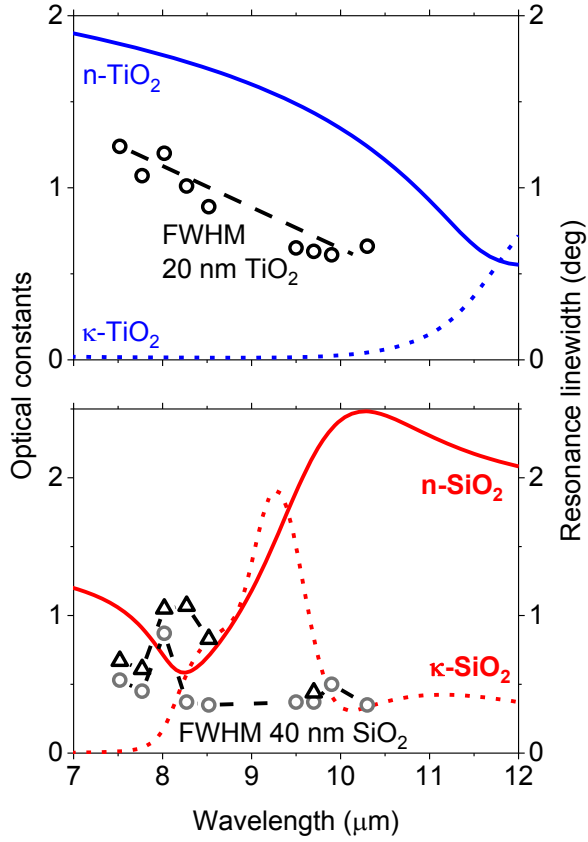

Figure 3. Resonance line width and spectrum of optical constants for dielectrics TiO_2 and SiO_2.

DISCUSSION

Figure 2 (right) shows that for SiO_2 thickness beyond about 100 nm, the absorption feature is so strongly broadened, that it no longer has the appearance of a resonance line. Figure 2 (left) shows that for 80 nm TiO_2 thickness, the resonance is already strongly broadened. For such resonances, the typical shifts in resonance angle that enable commercial plasmonic sensors [1], would be difficult to observe. Thus, we may say that, for SPP grating couplers with corrugations isolated from ground plane by dielectric, useful excitation resonances for traveling SPPs exist only up to a dielectric physical thickness of about 1% of the incident wavelength.

For TiO_2 the FWHM appears to decrease proportionally to the decrease the index spectrum in Figure 3. However, the change in FWHM is opposite the small changes in extinction coefficient, which is close to zero at all the measured wavelengths. The extinction coefficient for TiO_2 is also much smaller than that of SiO_2 in the 8-10 μm wavelength range, but the FWHM for TiO_2-based devices is much larger than that for SiO_2-based devices with the same dielectric thickness. Thus, resonance FWHM seems to be determined more by the index than by the extinction coefficient.

For SiO_2, the dependence of FWHM on wavelength is non-monotonic. Figure 3 shows that any possible correlation with the changes with index is more ambiguous than it is for TiO_2-based samples. There is apparently no correlation with the extinction coefficient spectrum of SiO_2.

It makes sense that resonances should broaden as index increases. A larger index increases the *optical* distance between grating and ground plane, which broadens the resonance in the same way as increasing the *physical* distance at a given wavelength for a given dielectric. Increased optical or physical distance both decrease the ability of electric induction to excite SPPs.

FDTD electrodynamic simulations were performed for the given device structure as a function of wavelength at fixed angle of incidence for six dielectric thicknesses up to 200 nm [10]. The simulation results agree with corresponding experiments performed using continuous wavelength sweep of the QCLs. We chose to present here only the subset of the data for the different configuration of variable angle and fixed wavelength, which is the most similar to commercial plasmonic sensors [1]. No simulations were performed for this configuration. However, we have shown elsewhere [11] excellent agreement between simulation and grating-coupler angular reflectance spectra. The agreement is even better when actual fabricated grating profiles are used as simulation input, but then the simulations take longer than is required to make and characterize a physical sample.

The Figure 1 structure is similar to MIM resonators that have been investigated for the last decade at near-IR [12-19], mid-wave IR [20-28], LWIR [9, 29], THz [30-35], and microwave wavelengths [36]. We cite here only MIM examples that resemble Figure 1, with continuous ground plane and simple metal patches on the surface, but our comments apply similarly to numerous examples of more complex MIM structures in the literature, e.g. [37]. The nature of the traveling-wave SPP excitation resonances investigated here is very different from the resonances observed in MIM devices. Our simulated field distribution images for traveling SPPs on grating surfaces [38] and for standing wave SPPs within MIM structures by ourselves [34] and many others inform and validate some of the contrasts presented next.

In MIM devices, the resonances are due to standing waves that are highly localized underneath the metal patches within sub-wavelength dimensions. The resonances change hardly at all with incidence angles over a wide range. Strong dielectric dispersion features cause additional resonances to appear [9, 35]. Resonance wavelengths are several times larger than the lateral dimensions of the top-metal patches. The resonance wavelengths are independent of periodicity [23, 27-29]. Absorption line widths depend

weakly on dielectric thickness. Absorption strength is optimized (usually by simulation, but in one case experimentally for three dielectrics [35]) at dielectric thicknesses from 0.6 to 15% of the resonance wavelength.

The traveling wave SPP resonances observed on the Figure 1 structure differ dramatically from MIM resonances in a number of ways. The fields of the inhomogeneous infrared waves extend a considerable distance above the surface in comparison to the wavelength. The resonance wavelengths are strongly dependent on incidence angle. Dispersion affects mainly the resonance line width but does not introduce new resonances. Resonance wavelengths (and angles) are mainly determined by the grating periodicity and not by the lateral dimensions of the metal stripes. Absorption lines widths broaden rapidly with increasing (optical and physical) dielectric thickness. Absorption strength is optimized for a dielectric thickness of zero.

Excitation of traveling SPPs at 15 μm wavelength has been reported on a 2D *semiconducting* grating separated from a *semiconducting* ground plane by SiO_2 dielectric of thickness 0.8 μm, which is 5% of the free space wavelength [39]. This interpretation contrasts with the experimental limits determined here. Perhaps the difference is in the lower plasma frequency of these conductors, which is a question worth systematic investigation.

A motivation for this work was infrared surface plasmon resonance biosensing. Only one type exists commercially, from a number of companies, and is in wide use by biologists [1]. For this type, sensing is based on the shift in a sharp excitation resonance angle for traveling SPPs. There are many academic (non-commercial) investigations of proposed infrared biosensors using surfaces with sub-wavelength metal structures that support localized, non-traveling SPPs, whose resonance wavelengths shift at constant incidence angle, e.g. [40-42]. These generally ignore the significant practical problems of exciting through an aqueous medium with interference by flow-channel hardware.

SUMMARY

SPPs can be excited on electrically-discontinuous gratings, provided a conducting ground plane is sufficiently near the isolated grating bars. The physical thickness of the isolation dielectric layer needs to be less than 1% of the wavelength to obtain a surface plasmon resonance excitation that is sufficiently narrow for sensor methodologies based on a shift in resonance angle at fixed wavelength. The resonance line width also depends on the *optical* thickness, i.e. on the refractive index, but the data do not support a dependence of resonance width on the dielectric extinction coefficient.

ACKNOWLEDGMENTS

University of Central Florida authors received partial support from AFRL contract FA8650-16-C-1738. Justin Cleary and Evan Smith acknowledge support from the Air Force Office of Scientific Research (Program Officer Dr. Gernot Pomrenke) under award number FA9550-19RYCOR048.

JRB would like to thank the Air Force for the support of this project though use of their clean room and IR characterization equipment, in addition to monetary support.

REFERENCES

1. Nico J. de Mol, Marcel J. E. Fischer, "Surface Plasmon Resonance: A General Introduction" in Surface Plasmon Resonance, Methods and Protocols, edited by Nico J. Mol, Marcel J. E. Fischer (Springer Humana, 2010), pp. 1-14.
2. R. Peale, J. Cleary, D. Shelton, G. Boreman, R. Soref, W. Buchwald, "Silicides for Infrared Surface Plasmon Resonance Biosensors," Proc. Mat. Res. Soc. 1133-AA10-03 (2008).
3. J. W. Cleary, G. Medhi, R. E. Peale, W. R. Buchwald, O. Edwards, and I. Oladeji, "Infrared Surface Plasmon Resonance Biosensor," Proc. SPIE 7673, 5 (2010).
4. D. M. Riffe, L. M. Hanssen, A. J. Sievers, Y. J. Chabal, and S. B. Christman, "Linewidth of H chemisorbed on W(100): An infrared study," Surf. Sci. 161, L559 (1985).
5. J. W. Cleary, G. Medhi, R. E. Peale, and W. R. Buchwald, "Long-wave infrared surface plasmon grating coupler," Appl. Optics 49, 3102 (2010).
6. W. L. Wolfe, "Optical materials," in Handbook of Military Infrared Technology, W. L. Wolfe, ed. (Office of Naval Research, Washington D.C., 1965).
7. D. A. Cardimona and D. H. Huang, "New optical detector concepts for space applications," Proc. SPIE 7679, 767903 (2010).
8. M. Vahdani, S. Yaraghi, H. Neshasteh, M. Shahabadi, "Narrow-Band 4.3μm Plasmonic Schottky-Barrier Photodetector for CO_2 Sensing," Sensors Letters 3, 3500504 (2019)
9. S. R. Calhoun, V. C. Lowry, R. Stack, R. N. Evans, J. R. Brescia, C. J. Fredricksen, J. Nath, and R. E. Peale, "Effect of dispersion on metal-insulator-metal infrared absorption resonances," MRS. Comm. 8, 830 (2018).
10. Jonathan Brescia, Grating Coupler for Surface Waves Based on Electrical Displacement Currents, Undergraduate Honors Thesis (UCF, Orlando, 2018).
11. R. Gibson, S. Vangala, I. O. Oladeji, E. Smith, F. Khalizadeh-Rezaie, K. Leedy, R. E. Peale, and J. W. Cleary, "Conformal spray-deposited fluorine-doped tin oxide for mid- and long-wave infrared plasmonics" Optical Materials Express 7, 2477 (2017).
12. C. Wu, Y. Avitzour, and G. Shvets, "Ultra-thin wide-angle perfect absorber for infrared frequencies," Proc. SPIE, 7029, 70290W (2008).
13. J. Hao, J. Wang, X. Liu, W. J. Padilla, L. Zhou, and M. Qiu "High performance optical absorber based on a plasmonic metamaterial," Appl. Phys. Lett. 96, 251104 (2010).
14. N. Liu, M. Mesch, T. Weiss, M. Hentschel, and H. Giessen, "Infrared perfect absorber and its application as plasmonic sensor," Nano Lett. 10, 2342 (2010).
15. J. Hao, J. Wang, X. Liu, W. J. Padilla, L. Zhou, and M. Qiu, "High performance optical absorber based on a plasmonic metamaterial," Appl. Phys. Lett. 96, 251104 (2010).
16. C. Wu, B. Neuner III, J. John, A. Milder, B. Zollars, S. Savoy, and G. Shvets, "Large-area wide-angle spectrally selective plasmonic absorber," Phys. Rev. B, 84, 075102 (2011).
17. B. Zhang, Y. Zhao, Q. Hao, B. Kiraly, I.-C. Khoo, S. Chen, and T. J. Huang, "Polarization-independent dual-band infrared perfect absorber based on a metal–dielectric–metal elliptical nanodisk array," Opt. Express 19, 15221 (2011).
18. C. Wu and G. Shvets, "Design of metamaterial surfaces with broadband absorbance," Opt. Lett. 37, 308 (2012).
19. H. M. Lee and J. C. Wu, "A wide-angle dual-band infrared perfect absorber based on metal–dielectric–metal split square-ring and square array," J. Phys. D 45, 205101 (2012).

20. M. Diem, T. Koschny, and C. M. Soukoulis, “Wide-angle perfect absorber/thermal emitter in the terahertz regime,” Phys. Rev. B 79, 033101 (2009).

21. X. Liu, T. Starr, A. F. Starr, and W. J. Padilla, “Infrared spatial and frequency selective metamaterial with near-unity absorbance,” Phys. Rev. Lett. 104, 207403 (2010).

22. Z. H. Jiang, S. Yun, F. Toor, D. H. Werner, and T. S. Mayer, “Conformal dual-band near-perfectly absorbing mid-infrared metamaterial coating,” ACS Nano 5, 4641 (2011).

23. C. W. Cheng, M. N. Abbas, C. W. Chiu, K. T. Lai, M. H. Shih, and Y.-C. Chang, “Wide-angle polarization independent infrared broadband absorbers based on metallic multi-sized disk arrays,” Opt. Express 20, 10376 (2012).

24. H. Cheng, S. Chen, H. Yang, J. Li, X. An, C. Gu, and J. Tian, “A polarization insensitive and wide-angle dual-band nearly perfect absorber in the infrared regime,” J. Opt. 14, 085102 (2012).

25. D. Cheng, J. Xie, H. Zhang, C. Wang, N. Zhang, and L. Deng, “Pantoscopic and polarization-insensitive perfect absorbers in the middle infrared spectrum,” J. Opt. Soc. Am. B 29, 1503 (2012).

26. J. Hendrickson, J. Guo, B. Zhang, W, Buchwald and R. Soref, “A wide-band perfect light absorber at mid-wave infrared using multiplexed metal structures,” Optics Letters 37, 371 (2012).

27. J. Nath, D. Panjwani, F. Khalilzadeh-Rezaie, M. Yesiltas, E. M. Smith, J. C. Ginn, D. J. Shelton, C. Hirschmugl, J. W. Cleary, R. E. Peale, “Infra-red spectral microscopy of standing-wave resonances in single metal-dielectric-metal thin-film cavity,” Proc. SPIE 9544, 95442M (2015).

28. A. Lefebvre, D. Costantini, I. Doyen, Q. Lévesque, E. Lorent, D. Jacolin, J-J. Greffet, S. Boutami, and H. Benisty: CMOS compatible metalinsulator-metal plasmonic perfect absorbers. Opt. Mater. Express 6, 2389 (2016).

29. J. A. Mason, S. Smith, and D. Wasserman, “Strong absorption and selective thermal emission from a midinfrared metamaterial,” Appl. Phys. Lett. 98, 241105 (2011).

30. Y. Q. Ye, Y. Jin, and S. He, “Omnidirectional, polarization insensitive and broadband thin absorber in the terahertz regime,” J. Opt. Soc. Am. B 27, 498 (2010).

31. Y. Ma, Q. Chen, J. Grant, S. C. Saha, A. Khalid, and D. R. S. Cumming, “A terahertz polarization insensitive dual band metamaterial absorber,” Opt. Lett. 36, 945 (2011).

32. X.-J. He, Y. Wang, J. Wang, T. Gui, and Q. Wu, “Dual-band terahertz metamaterial absorber with polarization insensitivity and wide incident angle,” Progress Electromagn. Res. 115, 381 (2011).

33. L. Huang, D. R. Chowdhury, S. Ramani, M. T. Reiten, S.-N. Luo, A. J. Taylor, and H.-T. Chen, “Experimental demonstration of terahertz metamaterial absorbers with a broad and flat high absorption band,” Opt. Lett. 37, 154 (2012).

34. J. Nath, S. Modak, I. Rezadad, D. Panjwani, F. Rezaie, J. W. Cleary, and R. E. Peale, “Far-infrared absorber based on standing-wave resonances in metal-dielectric-metal cavity,” Optics Express 23, 20366 (2015).

35. R. N. Evans, S. R. Calhoun, J. R. Brescia, J. W. Cleary, E. M. Smith, and R. E. Peale, “Far-infrared bands in plasmonic metal-insulator-metal absorbers optimized for long-wave infrared,” MRS Advances 4, 667 (2019).

36. M. J. Lockyear, A. P. Hibbins, J. R. Sambles, P. A. Hobson, and C. R. Lawrence, “Thin resonant structures for angle and polarization independent microwave absorption,” Appl. Phys. Lett. 94, 041913 (2009).

37. N. I. Landy, S. Sajuyigbe, J. J. Mock, D. R. Smith, and W. J. Padilla, “Perfect Metamaterial Absorber,” Phys. Rev. Lett. 100, 207402 (2008).

38. J. W. Cleary, G. Medhi, M. Shahzad, I. Rezadad, D. Maukonen, R. E. Peale, G. D. Boreman, S. Wentzell, and W. R. Buchwald, “Infrared surface polaritons on antimony,” Optics Express 20, 2693 (2012).

39. K. Gorgulu, A. Gok, M. Yilmaz, K. Topalli, N. Bıyıklı, Ali K. Okyay, “All-Silicon Ultra-Broadband Infrared Light Absorbers,” Scientific Reports 6, 38589 (2016).

40. F. B. Barho, F. Gonzalez-Posada, M-J. Milla-Rodrigo, M. Bomers, L. Cerutti, and T. Taliercio, “All-semiconductor plasmonic gratings for biosensing applications in the mid-infrared,” Optics Express 24, 16175 (2016).

41. R. Adato A. A. Yanik, J. J. Amsden, D. L. Kaplan, F. G. Omenetto, M. K. Hong, S. Erramilli, and H. Altug, “Ultra-sensitive vibrational spectroscopy of protein monolayers with plasmonic nanoantenna arrays,” PNAS 106, 19227 (2009).

42. D. Rodrigo, O. Limaj, D. Janner, D. Etezadi, F. J. García de Abajo, V. Pruneri, H. Altug, “Mid-infrared plasmonic biosensing with graphene,” Science 349, 165 (2015).